Materials Science and Engineering C 49 (2015) 297–304

Contents lists available at ScienceDirect

Materials Science and Engineering C

journal homepage: www.elsevier.com/locate/msec

Graphene–gold nanoparticle composite: Application as a good scaffold for construction of glucose oxidase biosensor

Sina Sabury [a], Sayed Habib Kazemi [b,*], Farhad Sharif [a]

[a] Department of Polymer Engineering and Color Technology, Amirkabir University of Technology, Tehran, Iran
[b] Department of Chemistry, Institute for Advanced Studies in Basic Sciences (IASBS), Zanjan 45137-66731, Iran

ARTICLE INFO

Article history:
Received 21 August 2014
Received in revised form 6 December 2014
Accepted 6 January 2015
Available online 8 January 2015

Keywords:
Reduced graphene
Gold nanoparticles
Biosensor
Glucose oxidase

ABSTRACT

In the present work we report a facile method for fabrication of glucose oxidase immobilized on the partially reduced graphene–gold nanocomposite (PRGO–AuNPs/GOx) as a novel biosensor for determination of glucose concentration. Scanning electron microscopy (SEM) and transmission electron microscopy (TEM) were used to study the morphology of PRGO and PRGO–AuNPs. Also, fast Fourier transformation infrared spectroscopy (FTIR) and UV–Vis spectroscopy were used to confirm formation of graphene and graphene–gold composite. Then, the electrochemical behavior of PRGO–AuNPs/GOx modified electrode was studied by cyclic voltammetry (CV). Our electrochemical studies, especially chronoamperometry (CA), showed that the PRGO–AuNPs/GOx modified electrode has excellent electrocatalytic activity towards the glucose. The limit of detection and sensitivity towards glucose were estimated as 0.06 μM and 15.04 mA mM^{-1}, respectively.

© 2015 Elsevier B.V. All rights reserved.

1. Introduction

Diagnosis of diabetes as its importance and universality needs great attention with precise monitoring of glucose level [1–3]. The typical method for monitoring glucose level from finger sticks may be painful, in addition to its relatively high cost, which needs more infection cares. Since the glucose level in the blood has linear dependency to its level in saliva, this may lead to an alternative non-invasive self-measurement of glucose level. Glucose level in human saliva for healthy body is in the range of 8–210 μM compared to blood glucose level (4–8 mM) [4,5]. Low glucose level (hypoglycemia) symptoms occur below this value (from 0.92 to 1.63 μM for salivary flow as average in diabetic patients [6]). Most of the existing biosensors work in milli-molar range, so micro-molar sensing of glucose level in biofluid with high sensitivity has attracted great importance [5,7]. Glucose enzymatic sensing based on glucose oxidase (GOx) has been commonly used due to its high sensitivity; selectivity and low detection limit [8–12]. There are several methods to determine the glucose concentration in which GOx catalyzes the reaction of glucose with oxygen and yield oxidized form of glucose. One of the most important methods to determine the glucose concentration includes oxygen measurement [13,14]. However, due to oxygen dissolution difficulties, detection of glucose concentration based on the detection of hydrogen peroxides (H_2O_2) as a product of the glucose oxidation reaction has been proposed. Hydrogen peroxide has relatively high overpotential against standard cells [15,16]. Probabilities of oxidation of the species during electrochemical measurements lead to comprehensive studies on electron transfer between enzyme and electrode surface. Effective immobilization of enzyme is a crucial issue to accomplish sufficient electrical communication between enzyme and electrode surface [17–22]. Various materials and methods have been developed to immobilize enzyme, including nanostructures like conducting polymers, carbon nanotubes (CNTs), graphene, metal and metal oxide nanoparticles [11,16,23–30]. It was observed that functionalized surface can affect the immobilization efficiency [31,32]. Recently, CNTs were investigated to immobilize the enzyme and the corresponding results confirm the importance of introducing appropriate functionalities [31,33]. Consequently, introducing a wide variety of functional groups especially carboxylic acid group has been studied [11,33,34]. Moreover, coupling of amino derivative group of glucose cofactor, Flavin Adenine Dincleotide (FAD), with carboxylic acid moiety has been well defined [10,11,28,33,34]. Of note, the enzyme active sites must be positioned efficiently in close vicinity to the electrode surface for effective electron transfer [31,34]. Also, it is proved that electrical conductivity and biocompatible microenvironment matrix is an essential need for biosensing purposes.

Graphene as an atom-thick two dimensional honeycomb carbon structure with high electrical conductivity, large active surface area, rapid electron transfer and good biocompatibility; has attracted great interests in bioelectrochemistry [8,22,25,35–37]. It was reported that the chemically reduced graphene oxide (RGO) may experience irreversible restacking because of van der Waals and πi–πi interactions, resulting in difficulties in processability and decrease in active surface area.

To prevent single graphene sheets from agglomeration in dry state, also addition of synergic effect of catalytic properties, conducting

* Corresponding author.
E-mail address: habibkazemi@iasbs.ac.ir (S.H. Kazemi).

http://dx.doi.org/10.1016/j.msec.2015.01.018
0928-4931/© 2015 Elsevier B.V. All rights reserved.

biocompatible nanostructures such as gold nanoparticles has been used [38,39]. Fabrication of Au nanoparticles (AuNPs) and graphene sheet composite is conducted through two main methods. The first method includes using an intermediate as linker between AuNPs and graphene [40–42]. Cao et al. have employed cationic polyelectrolyte protected AuNPs in order to immobilize glucose oxidase using a layer-by-layer method [43]. The decrease in conductivity of composite due to the presence of insulting materials has been reported as a major disadvantage in this method. The second method is in-situ synthesis of graphene–AuNP composite through co-reduction of graphene oxide and Au salt [44]. Cui and Zhang have fabricated graphene–AuNP composite to use in electrochemical sensor to determine the epinephrine concentration [40]. However, there are some limitations to the second method which are still challenging. The main challenges are difficulties to control the reduction process, homogeneous distribution of nanoparticles, and ability to control the morphology of AuNPs and the more important problem is lack of good processability. Low processability occurs since the resulting composite yield in the form of precipitate and biosensing applications requires dispersed materials [41,45]. It should be noted that intercalation of metal nanoparticles between reduced graphene oxide sheets may not happen in the abovementioned approaches. However, stability of graphene oxide in the presence of specific ionic strength is still under investigation [46–48].

Herein, we employed the optimum conditions of graphene reduction to maintain the conductivity of graphene sheets while keeping some of useful graphene oxide functionalities to ensure communication of enzyme with electrode surface. Keeping the functional groups helps to form stable colloid and provides homogeneous mixing of AuNPs and PRGO without any macromolecular additive. The stability of the colloids also improves processability and ease of casting of PRGO–AuNPs on glassy carbon electrode (GCE). In the present work, AuNPs and PRGO were synthesized separately by a well-defined method via $HAuCl_4$ reduction using sodium citrate. Condensation reaction between amino group moiety of enzyme and carboxylic group of PRGO enhances the kinetics of electron transfer.

2. Experimental

2.1. Materials

Glucose oxidase, hydrazine hydrate, and graphite powder were purchased from Sigma-Aldrich Company and used as received. Other chemicals were purchased from Merck Company and used without further purification. All solutions were prepared by using ultrapure water from a Millipore-MilliQ system. All the experiments were performed at ambient temperature.

2.2. Apparatus

All electrochemical experiments were carried out using an EG&G potentiostat–galvanostat (model 263-A, USA) equipped with Power Suite software package. Electrochemical studies were performed using a conventional three-electrode cell. A 3 mm modified GCE electrode, an Ag/AgCl and a platinum rod were used as working, reference and counter electrodes, respectively. All potentials were measured and reported against the Ag/AgCl reference electrode.

Scanning electron microscopy (SEM) was performed by Seron AIS2100, using 15 kV accelerating voltage. Transmission electron microscopy (TEM) was performed by a LEO 912AB electron microscope at 150 kV. Samples were prepared without gold coating due to sufficient conductivity. At first, samples were dried out at room temperature to avoid any excess reduction; then mixed with KBr to obtain test samples for FT-IR spectroscopy. The IR spectra were obtained from 400 to 4000 cm^{-1} with a resolution of 4 cm^{-1} by a Nicolet-IR100 spectrometer. UV–Vis spectra were obtained using a Cecil CE9200, England.

2.3. Synthesis of GO and PRGO

GO was synthesized from graphite flake using modified Hummers method [49]. Briefly, 1 g of natural graphite powder and 0.5 g of $NaNO_3$ were added to 40 ml of H_2SO_4 solution and the resulting mixture was allowed to stir for 30 min (mild pre-oxidation step). Then, 4 g of $KMnO_4$ was added to this mixture and left it at 30 °C for 120 min, to form a paste. In the next step, 200 ml of water and 17 ml of H_2O_2 solution (30 wt.%) were added to the mixture to obtain graphite oxide mixture. The graphite oxide mixture was then centrifuged and washed three times with a 1.0 M HCl solution and water. Finally, the resulting solution was sonicated (CD-4820 40W) for 30 min to produce graphene oxide dispersion.

In order to yield stable dispersion of partially reduced graphene oxide (PRGO), chemical reduction with hydrazine was applied through the procedures suggested by Li and co-workers [50]. Briefly, GO dispersion was diluted to 0.5 mg/ml. Then, 85 ml of as-prepared dispersion was mixed with 0.06 ml of hydrazine (55% wt in water). The weight ratio of hydrazine to GO was controlled at 0.7. Also, pH was adjusted with adding appropriate amount of ammonia solution (28 wt.% in water) to convert carboxylic acid group to the corresponding carboxylate form. The mixture was stirred using a magnetic stirrer for 10 min, then it was put in a 95 °C water bath for 1 h. The stable PRGO dispersion was yielded after removing the black precipitates via glass cotton filtration. Scheme 1 displays the GO and PRGO synthesize route.

2.4. Synthesis of AuNPs and PRGO–AuNPs

Colloidal AuNPs were prepared according to the literature by reaction of sodium citrate solution and $HAuCl_4$ solution which was previously heated up to 60 °C. Briefly, 0.5 ml of 1% (w/v) sodium citrate solution as reducing agent was added dropwise to 50 ml of 0.01% (w/v) $HAuCl_4 \cdot 3H_2O$. The resulting mixture was boiled for 15 min. Then, the prepared stable colloid was stored in dark glass bottle at 4 °C. Additionally, stable dispersion of AuNPs was added to PRGO colloid with concentration of 0.5 mg ml^{-1} and mixed in a shaker for overnight to ensure the complete intercalation of nanoparticles between PRGO sheets. The weight ratio of AuNPs to PRGO was adjusted at 1. Scheme 2 is a simple representation of the applied strategy for preparation of PGRO–AuNPs.

2.5. Preparation of PRGO–AuNPs–GOx–GCE

At first, a GC electrode was polished with 0.5 and 0.05 μm Al_2O_3 powder to reach to the mirror finish surface. Then, it was rinsed with water and sonicated in ethanol and doubly distilled water. The cleansed GCE was gently dried under a nitrogen atmosphere. In the next step, 5 μl of PRGO–AuNP composite (1 mg ml^{-1}) was dropcasted on GCE, and then it was left in room temperature to evaporate its solvent. Finally, 2 μl of GOx solution (10 mg ml^{-1}) was dropcasted on the PRGO–AuNP modified electrode. The fabricated PRGO–AuNPs–GOx electrode was rinsed with ultrapure water to wipe off any loosely attached GOx. In a control experiment, to check the effects of AuNPs, the similar procedure was repeated to modify a GCE in which pure PGRO was dropcasted on the electrode. These two modified electrodes were denoted as PRGO–AuNPs–GOx and PRGO–GOx, respectively. The voltammetric behavior of PRGO–AuNPs–GOx and PRGO–GOx modified electrodes was investigated at various pH (from 5.8 to 8) by cyclic voltammetry at a scan rate of 100 mV s^{-1} in the air saturated condition. To determine the glucose concentration, electrochemical tests were performed in 0.1 M of phosphate buffer solution (PBS). Scheme 3 is a graphical representation of the abovementioned procedures.

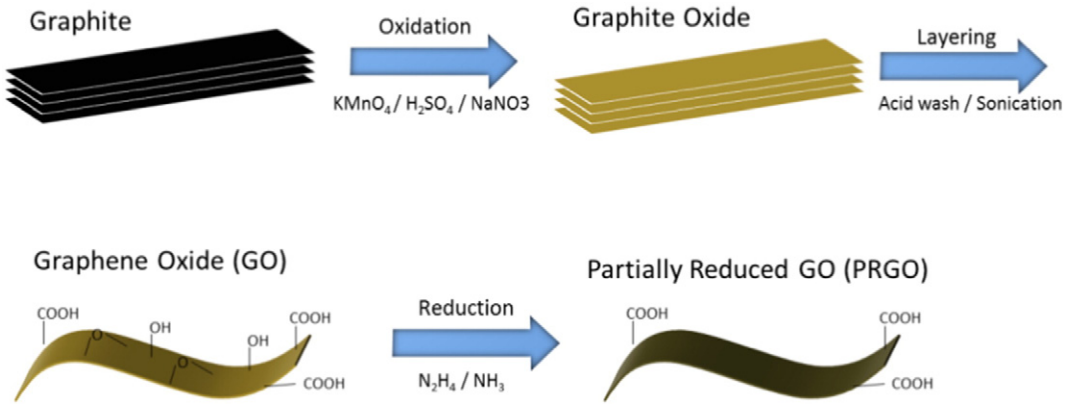

Scheme 1. Schematic diagram of synthesizing the GO and PRGO.

3. Result and discussion

3.1. Characterization of PRGO–AuNPs

Fig. S1 (Supplementary information) shows FT–IR spectrum of synthesized GO produced from oxidation of graphite. Oxygen containing groups on GO surfaces can be confirmed by bands located at 3438, 1640 and 1031 cm^{-1}; indicating the stretching vibration of O–H, C═O, and C–O bond, respectively [51,52]. The morphology of GO product was characterized by SEM (Fig. 1). As shown in Fig. 1, crumpled layered GO and folded edges can be observed for GO compared to stacked structure of pristine graphite [53]. Reduction process of GO was monitored by UV–Vis absorption method. An important characteristic property of conjugated carbon atoms is π–π^* transition of C═C band; supported by an absorption peak around 230 nm [54]. Fig. 2 represents the reduced sample with a maximum absorption peak around 256 nm and this is raised from retained conjugated bonds in the carbon based backbone [41,54]. Higher red shifts observed for a maximum absorption peak (up to 280 nm) have been reported previously. Thus, this sample can be considered as partially reduced GO with partly restored conjugated electron path and partly remained oxygen containing functional groups [54]. The conjugated bonds play an important role in conductivity; and also the remaining functional groups are critical scaffolds for enzyme immobilization.

Fig. S2 (Supplementary information) represents stable aqueous colloids of GO and PRGO. High stability of reduced GO results in better processability and considerable electrical behavior; in addition to form homogeneous solution with a wide variety of materials [53,55]. Synthesized AuNPs were characterized by UV–Vis spectroscopy. The surface plasmon resonance band in the range of 520–540 nm is an evidence for a colloid solution of spherical gold nanoparticles. Fig. S3 (Supplementary information) displays absorption peak at 526 nm which is in agreement with previously reported works [56,57].

UV–Vis spectroscopy test was also employed to examine PRGO–AuNP colloid and depicted as Fig. 2. As seen in Fig. 2, characteristic absorbance bands of PRGO and AuNPs can be distinguished. It should be considered that a slight excess in reduction of PRGO may occur after encountering sodium citrate; resulting in a red shift from 256 to 264 nm for the characteristic band [54]. The morphology of PRGO–AuNP nanocomposite was studied by TEM (Fig. 3). TEM images demonstrate the

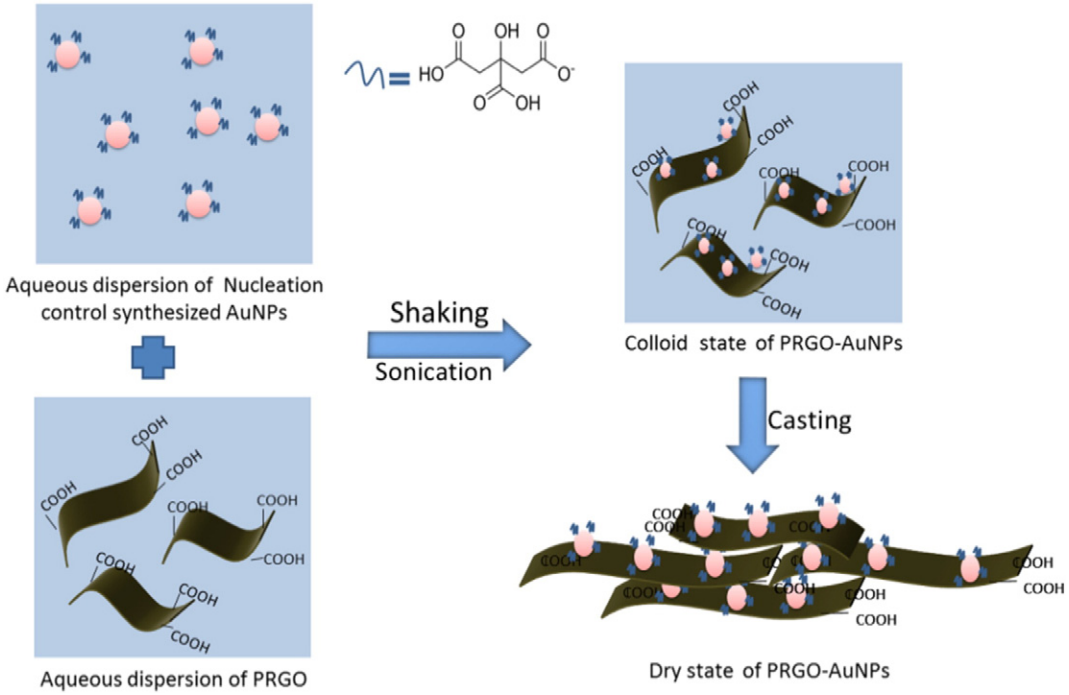

Scheme 2. Schematic diagram of fabricating the PRGO–AuNPs.

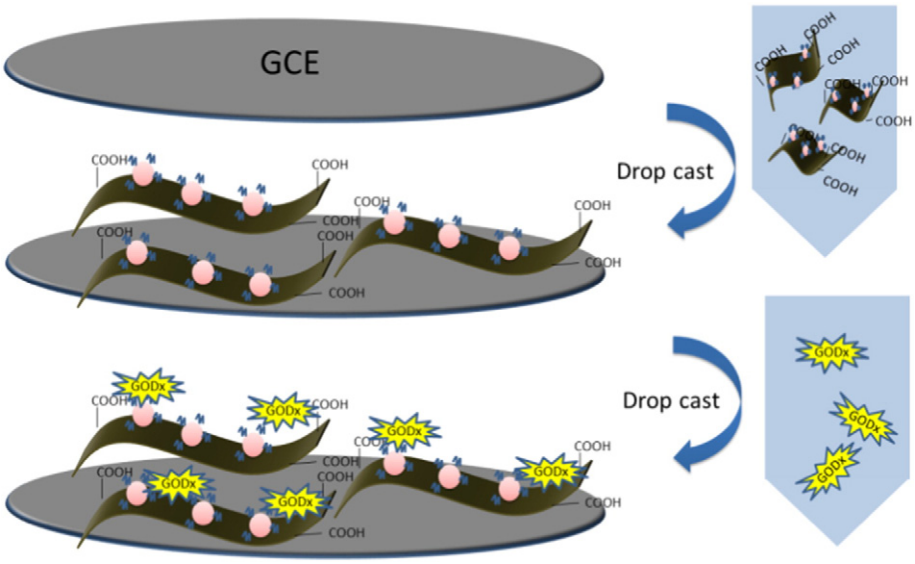

Scheme 3. Schematic diagram for preparation PRGO–AuNPs–GOx modified GC electrode.

relatively uniform distribution of AuNPs on PRGO surface. Also, air dried PRGO shows restacked morphology in comparison with nanoparticle intercalated composite. The particle size distribution analysis was done for TEM images using the *ImageJ* program (Fig. 4).

3.2. Electrochemical behavior of PRGO–AuNPs–GOx

To investigate the electrochemical behavior of PRGO–AuNPs and PRGO–AuNPs–GOx electrodes, cyclic voltammograms were recorded in PBS of PH = 7.0 at a scan rate of 100 mV s^{-1} (air saturated solution). The potential range was −0.55 to −0.35 V against Ag/AgCl, also the response of modified electrodes compared to the bare electrode voltammograms (shown in Fig. 5). As seen, there is no Faradaic peak for bare electrode in the potential range studied. It is observed that a sluggish electron transfer reaction may occur, as shown in Fig. 8. Compared to PRGO–AuNPs–GOx electrode, the peak shape and height are suppressed for both GO–GOx and PRGO–GOx modified GCE. Of note, GO–GOx voltammogram was nearly as same as PRGO–GOx. It has reported that due to the orientation of the FAD in the cleft, direct FAD oxidation by an electrode is kinetically unfavorable. After incorporation of gold nanoparticles, the electron transfer behavior becomes faster and facile, thus we conclude that the gold nanoparticles will act as electron relay between enzyme and graphene sheets due to their small size which allows communicating with enzyme active centers. It is observed that the formal potential for redox process of the GOx on AuNPs–PRGO modified surface is located at −0.44 V which is very close to the standard potential of FAD/$FADH_2$ couple (−0.46 V in pH 7.0). This evidence indicates the native structure of immobilized GOx on modified electrode surface [58]. It can be concluded that the absence of macromolecular additive, hence keeping the functional groups available for biosensor preparation results in formation of stable colloid and provides homogeneous mixing of AuNPs and PRGO. The stability of the AuNPs and PRGO colloids will advance the ease of casting of PRGO–AuNPs on glassy carbon electrode (GCE) without the need of any binder. Elimination of binder from the biosensor structure will also result in a lower charge transfer and ohmic resistance of electrode material. Furthermore, the peak potential difference between the anodic and cathodic peaks (ΔE_p) is approximately 17 mV; indicating the fast electron transfer kinetic due to facilitated direct electron transfer between FAD/$FADH_2$ redox couple and electrode [59,60].

3.3. Effect of pH on electrochemical properties of PRGO–AuNPs–GOx

The effect of pH on the redox behavior of immobilized GOx at the PGRO–AuNPs–GCE surface was investigated in a relatively wide pH range from 5.8 to 8.0 by cyclic voltammetry. As seen in Fig. 6, the cathodic peak current was increased with increase in pH from 5.8 to 7.0, and then it decreased by increasing pH from 7.0 to 8.0. It can be considered as a reason for pH dependency of the redox response of GOx on gold nanoparticles. The maximum cathodic current was obtained at pH 7.0, therefore it was chosen as the optimal pH for next experiments. Also, the results showed that the slope of E_{pc} against pH is 61.5 mV pH^{-1} over the applied pH range. This value was close to the theoretical Nernstian value of 59.2 mV for a two-electron, two-proton process

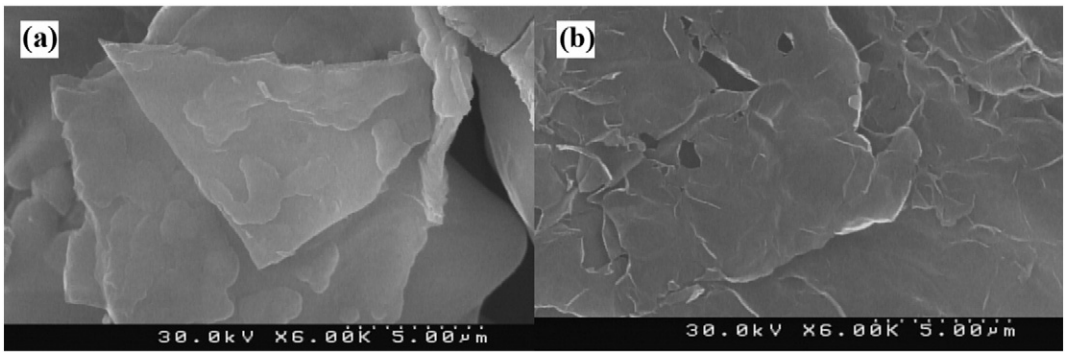

Fig. 1. SEM of (a) stacked structure of graphite powder, and (b) wrinkled GO layers.

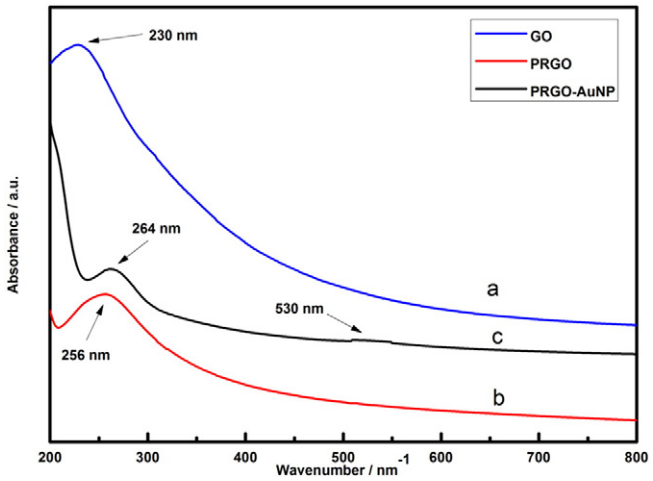

Fig. 2. UV–Vis absorption spectra of (a) GO, (b) PRGO, and (c) PRGO–AuNP nanocomposite.

found for GOx Faradaic behavior in previously reported works. The mechanism of electrocatalytic activity of GOx at the electrode surface is fairly well-known in which the main active center of enzyme, FAD, will reduce to $FADH_2$ by giving $2e^-/2H^+$ as below.

$$GOx\ (FAD) + 2H^+ + 2e^- \rightarrow GOx\ (FADH_2)$$

Thus, it is expected to see a slope of approximately 59.0 mV for E–pH plot data which is very close to 61.2 mV in the present work.

3.4. Effect of the scan rate on the electrochemical behavior of PRGO–AuNPs–GOx

One of the most important experiments to check the reversibility of a redox reaction is studying the response of the electrochemical system against the scan rate. Fig. 7A illustrates the voltammograms of PRGO–AuNPs–GOx modified electrode recorded at different scan rates ranging from 50 to 1000 mV s^{-1}. Moreover, both anodic and cathodic peak currents increased linearly with scan rate, as expected for surface-controlled redox reactions. Although the GOx redox reaction (FAD and $FADH_2$) is a quasi-reversible process, small value of ΔEp can be considered as an evidence for a relatively fast electron transfer (Fig. 7B).

In addition, the rate constant of the electrochemical reaction of FAD/$FADH_2$, k_s (s^{-1}), was estimated by using the Laviron equation at high rate conditions as [61]:

$$\log k_s = \alpha \log(1-\alpha) + (1-\alpha)\log\alpha - \log(RT/nF\vartheta) - \alpha(1-\alpha)nF\Delta E_p/2.3RT$$

where R is an ideal gas constant, T is the temperature in Kelvin; F is the Faraday's constant, υ is the potential scan rate, n is the number of electrons in redox reaction ($n = 2$), and ΔE_p is the difference between cathodic and anodic peak potentials. Also, charge transfer coefficient (α) is assumed to be approximately 0.5 for surface confined condition. The electron transfer rate constant (k_s) was determined to be 5.01 s^{-1}, which is an evidence for facile electron exchange kinetics through immobilized enzyme [58,60,61].

In addition, the surface concentration of redox species (FAD/$FADH_2$) was estimated using the slope of peak current against the potential scan rate [61]:

$$i_p = n^2F^2\vartheta A\Gamma/4RT$$

where Γ is the amount of GOx participated in reaction at enzyme covered electrode surface (mol cm^{-2}), A is the electrode area, υ is the scan rate, and also n, F, R and T have their usual value as mentioned before. The amount of electroactive GOx, Γ, is estimated as 1.80×10^{-11} mol cm^{-2} which is greater than its theoretical monolayer on the surface (6.35×10^{-13} mol cm^{-2}). This result suggests increasing electroactive surface area because of incorporation of AuNP flocks into the PRGO scaffold which is in good agreement with previously reported works [58,62].

3.5. Chronoamperometric detection of glucose

In order to check the electrocatalytic activity of modified electrode towards the glucose, hydrodynamic chronoamperometry was performed. The amperometric response of PRGO–AuNPs–GOx modified electrode at an optimized potential step of −0.45 V vs. reference electrode was recorded upon successive addition of glucose into cell solution. Also, corresponding amperometric plot for real sample spiking is provided as Fig. S4 (Supporting information). It was found that the amperometric current reached to the steady state within 5 s upon successive additions of glucose sample over a wide range of concentration. The amperometric response is linear against the concentration of glucose within 0.14 to 4.0 μM.

Using the linear regression method (Fig. 8), the limit of detection of glucose concentration (LOD) was estimated to be 0.060 (±0.001) μM (the regression equation was obtained as i(μA) = 0.11 × Conc. (μM) + 0.31 and analytical sensitivity of 0.115 μA μM^{-1}). Table 1 represents the comparison of PRGO–AuNPs–GOx modified electrode with some similar biosensors, reported previously for determination of glucose concentration. As seen, the electrochemical and analytical performance of the present biosensor is superior compared to these reported works. To check the interference effects of the most important interferences in biological media, especially ascorbic acid and urea, glucose determination analysis was performed in a synthetic real sample solution including these interferences, and we have found insignificant

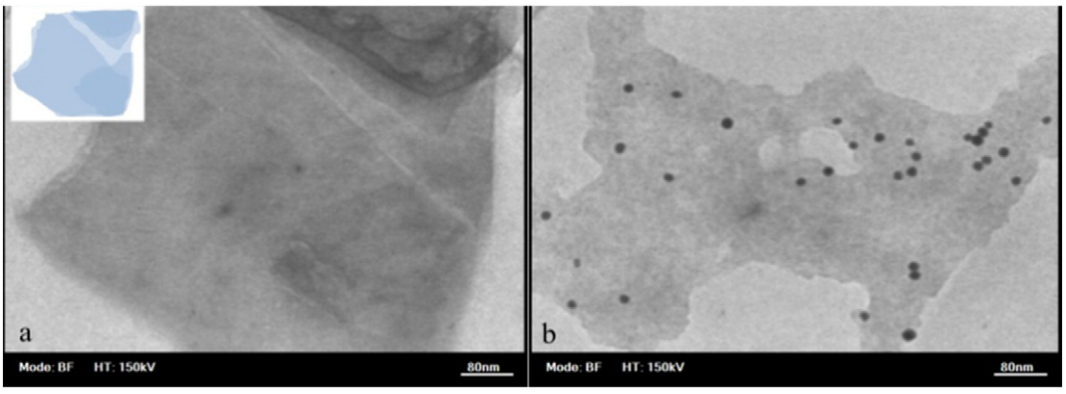

Fig. 3. TEM images of (a) drying induced multi-layered PRGO and its schematic representation (inset), (b) PRGO–AuNP nanocomposite.

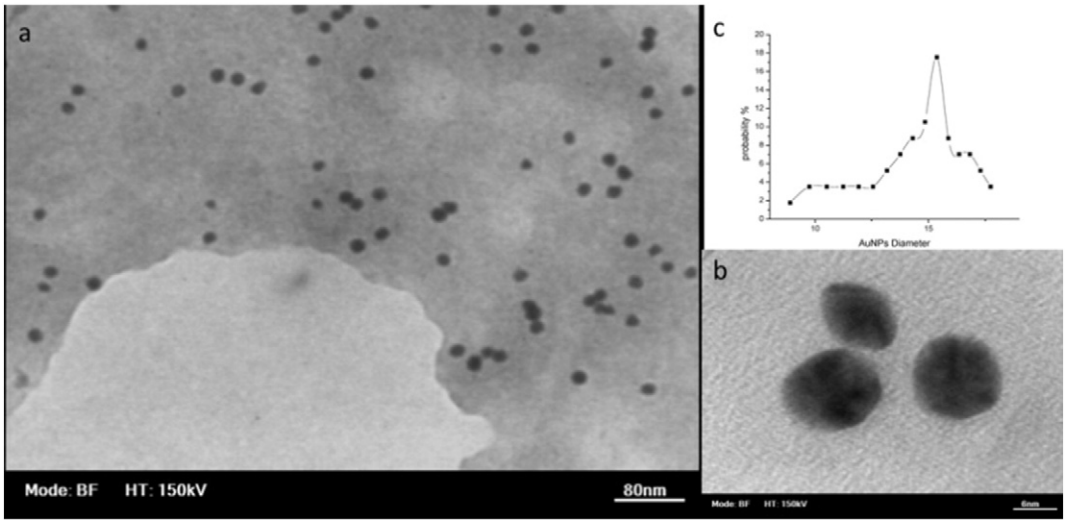

Fig. 4. (a) TEM images of AuNP particle distribution measuring sample, (b) high resolution image of AuNPs demonstrating the spherical shape of nanoparticles, (c) particle size distribution from *ImageJ* program.

changes in analytical performance of the biosensor at high concentrations (concentration of interferences was at least 100 times larger than the glucose concentration, Supplementary information Fig. S4). Corresponding amperometric plot for real sample spiking is provided as Fig. S4 (Supplementary information). Also, in a separate test, analysis of acid ascorbic and urea standard solutions at high concentrations was examined by spiking the synthetic real sample between glucose addition steps. Inconsiderable changes (less than 2.5%) were observed relative to current height occurred for addition of standard solution of glucose (shown as Fig. S5, Supplementary information).

Additionally, the electrode stability and reproducibility as important features of a biosensor were examined. To accomplish it, glucose determination analysis by amperometric method was performed in a time period of at least one month (each day signal recording was done), and it was found that the biosensor response only decreased 6% after two weeks. Thus, it was concluded that the biosensor stability is considerable. Moreover, successive cyclic voltammograms for PRGO–AuNPs–GOx electrode were recorded in PBS electrolyte and insignificant decrease in either peak current or peak potential (less than 3%) was observed after 100 cycles. Also, the relative standard error for such analysis was estimated as 2.5% for at least seven repetitive determination of glucose concentration using PRGO–AuNPs–GOx electrode. Considering the whole results provided, we suggest the PRGO–AuNPs–GOx electrode as reliable and suitable biosensor to determine the low level concentrations of glucose.

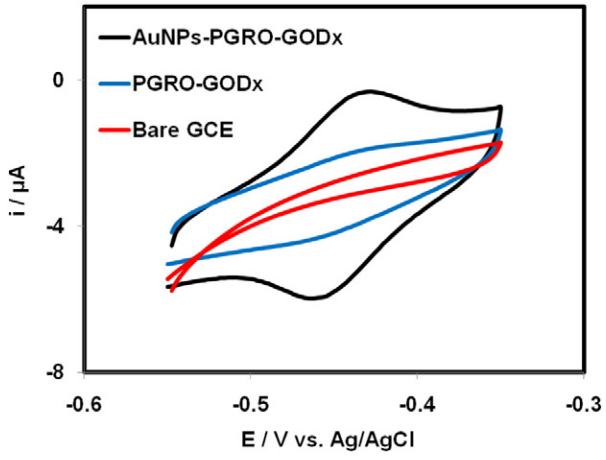

Fig. 5. Cyclic voltammograms recorded for Bare GC (red plot), PRGO–GOx/GC (blue), and PRGO–AuNPs/GOx/GC electrode (black) in 0.1 M pH 7 PBS. The scan rate is 100 mV/s at air saturated condition.

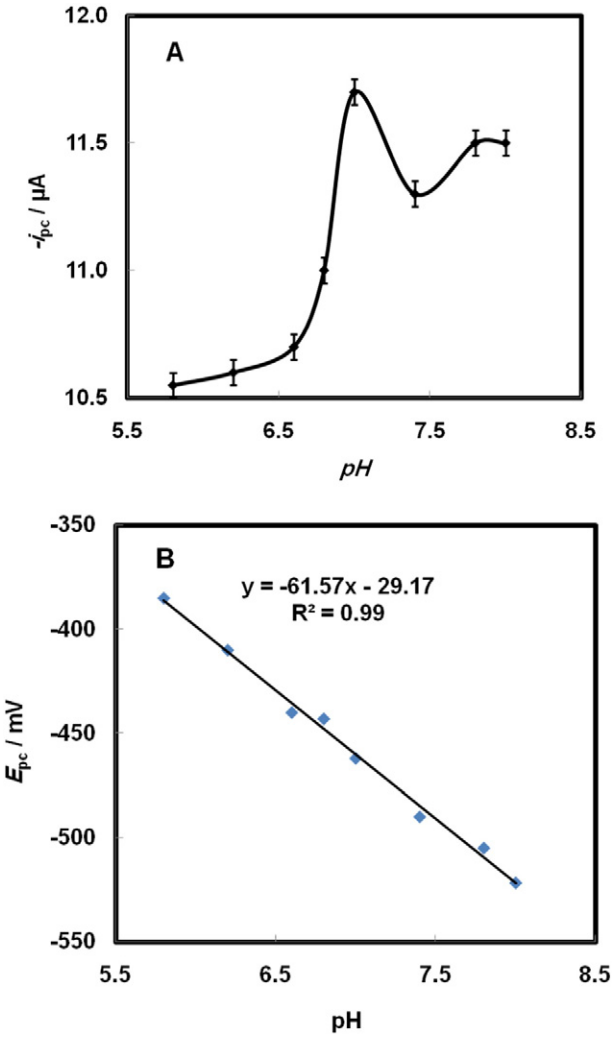

Fig. 6. (A) Plot of I_{pc} vs. pH of PRGO–AuNp/GOx/GC electrode in 0.1 M PBS at pH 6.2, 6.8, 7, 7.4, 7.6, 7.8 and 8.0, and (B) the plot of E_{pc} vs. pH.

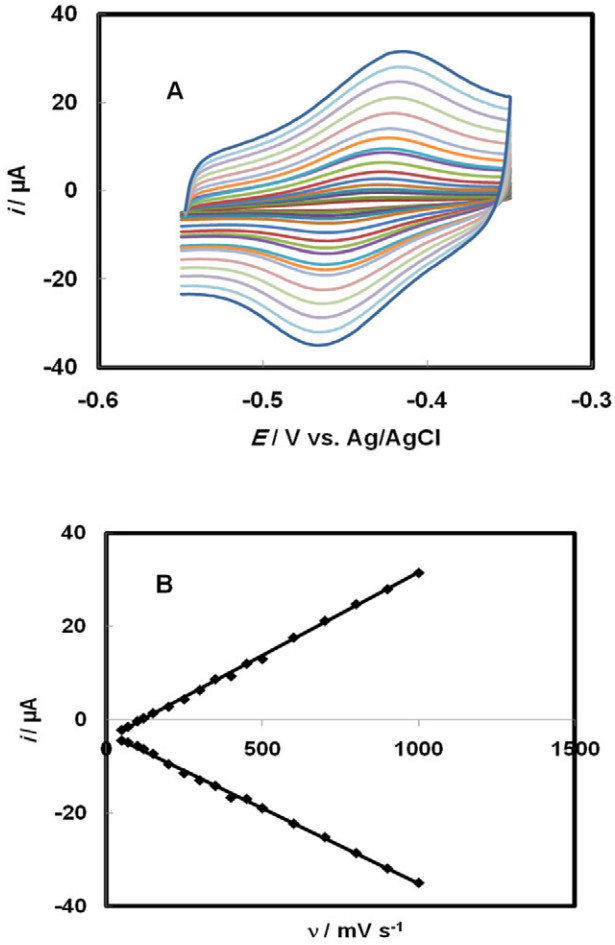

Fig. 7. A) Cyclic voltammograms recorded for PRGO–AuNp/GOx/GC electrode at different scan rates in 0.1 M pH 7 PBS at air saturated condition, B) the plot of I_p vs. scan rate for PRGO–AuNPs/GOx/GC electrode in 0.1 M phosphate buffer solution at pH 7.

4. Conclusions

We report a facile method to design a novel glucose biosensor using gold nanoparticles decorated reduced graphene as a reliable scaffold for enzyme immobilization. Our electrochemical studies revealed that the AuNPs enhanced the electron transfer behavior of the glucose oxidase. The PRGO–AuNPs–GOx modified electrode demonstrated good electrocatalytic activity towards the glucose oxidation reaction, thus it was used to determine the concentration of glucose. This biosensor presents excellent limit of detection and sensitivity towards glucose concentration. Also, it was found that the present biosensor can work in the presence of high concentration of ascorbic acid and uric acid as the most important interferences in the biological samples, especially blood serum. Thus, PRGO–AuNPs–GOx biosensor can be considered as a reliable candidate for determination of glucose concentration in biological samples for medical purposes.

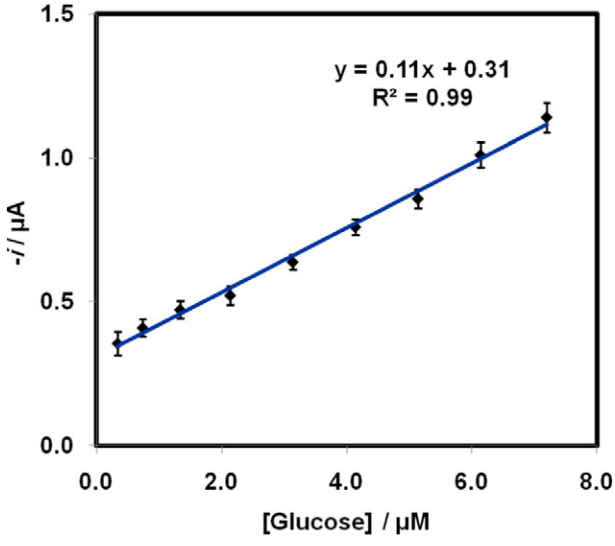

Fig. 8. Calibration curve for the PRGO–AuNPs/GOx/GC electrode recorded by chronoamperometry in 0.1 M pH = 7 of PBS against the glucose concentrations added.

Table 1
Comparison of analytical performance of PRGO–AuNPs/GOx biosensor with previously reported similar glucose biosensor.

Electrode	Linear range μM	LOD μM	Sensitivity μA μM^{-1}	E_{app}[a] vs. Ag/AgCl V	Ref.
GOx/AuNPs/Pb NW/Pt	5–2200	2	0.136	0.19	[63]
GOx/nafion/AuNPs–MWCNT[b]	50–22,000	20	0.0004	−0.5	[64]
Chitosan-GOx-AuNPs	5–2400	2.7	–	0.7	[65]
GOx/AuNPs–graphene–chitosan	2000–10,000	180	0.099	−0.2	[39]
GOx/RGO	100–27,000	–	1.85	−0.44	[60]
GOx/GO/MWCNT[b]	100–28,000	28	0.0026	−0.40	[66]
PPy[b]–GOx–RGO	2–40	3	–	0.2	[8]
GOx/PEDOT[b]/PtNP/graphene	10–50,000	0.3	–	–	[67]
GOx/ERGO[b]–AuNPs	200–2000	17	0.0569	0.39	[68]
GOx/PRGO–AuNPs	0.4–4	0.06	15.04	−0.445	This work

[a] Applied potential to biosensor.
[b] (MWCNT): Multiwall carbon nanotube, (PEDOT): poly 3,4-ethylenedioxythiophene, (PPy): polypyrrole, (ERGO): electrochemical reduced graphene oxide.

Acknowledgment

Supports of the work by Amirkabir University of Technology and Institute for Advanced Studies in Basic Sciences (Ministry of Science Research and Technology, MSRT, Iran) are acknowledged. Also, valuable comments of the reviewers are appreciated.

Appendix A. Supplementary data

Supplementary data to this article can be found online at http://dx.doi.org/10.1016/j.msec.2015.01.018.

References

[1] J.S. Hansen, J.B. Christensen, J.F. Petersen, T. Hoeg-Jensen, J.C. Norrild, Sensors Actuators B Chem. 161 (2012) 45–79.
[2] A. Heller, B. Feldman, Electrochemical glucose sensors and their application in diabetes management, Applications of Electrochemistry in Medicine, Springer, 2013. 121–187.
[3] A. Heller, B. Feldman, Acc. Chem. Res. 43 (2010) 963–973.
[4] M. Yamaguchi, M. Mitsumori, Y. Kano, IEEE Eng. Med. Biol. Mag. 17 (1998) 59–63.
[5] D.J. Macaya, M. Nikolou, S. Takamatsu, J.T. Mabeck, R.M. Owens, G.G. Malliaras, Sensors Actuators B Chem. 123 (2007) 374–378.
[6] C. Jurysta, N. Bulur, B. Oguzhan, I. Satman, T.M. Yilmaz, W.J. Malaisse, A. Sener, J. Biomed. Biotechnol. 2009 (2009).
[7] Y. Kostov, X. Ge, G. Rao, L. Tolosa, Meas. Sci. Technol. 25 (2014) 025701.
[8] S. Alwarappan, C. Liu, A. Kumar, C.-Z. Li, J. Phys. Chem. C 114 (2010) 12920–12924.
[9] X. Kang, J. Wang, H. Wu, I.A. Aksay, J. Liu, Y. Lin, Biosens. Bioelectron. 25 (2009) 901–905.
[10] F. Li, Z. Wang, C. Shan, J. Song, D. Han, L. Niu, Biosens. Bioelectron. 24 (2009) 1765–1770.
[11] Y. Lin, F. Lu, Y. Tu, Z. Ren, Nano Lett. 4 (2004) 191–195.
[12] M. Wooten, S. Karra, M. Zhang, W. Gorski, Anal. Chem. 86 (2014) 752–757.
[13] A.H. Kadish, R.L. Litle, J.C. Sternberg, Clin. Chem. 14 (1968) 116–131.
[14] J. Wang, Chem. Rev. 108 (2008) 814–825.
[15] W. Jia, M. Guo, Z. Zheng, T. Yu, E.G. Rodriguez, Y. Wang, Y. Lei, J. Electroanal. Chem. 625 (2009) 27–32.
[16] A. Salimi, R.G. Compton, R. Hallaj, Anal. Biochem. 333 (2004) 49–56.
[17] A. Sassolas, L.J. Blum, B.D. Leca-Bouvier, Biotechnol. Adv. 30 (2012) 489–511.
[18] D.N. Tran, K.J. Balkus Jr., ACS Catal. 1 (2011) 956–968.

[19] Y.-T. Wang, L. Yu, Z.-Q. Zhu, J. Zhang, J.-Z. Zhu, C.-h. Fan, Sensors Actuators B Chem. 136 (2009) 332–337.
[20] H. Wu, J. Wang, X. Kang, C. Wang, D. Wang, J. Liu, I.A. Aksay, Y. Lin, Talanta 80 (2009) 403–406.
[21] K. Zargoosh, M. Shamsipur, S. Hossienkhani, S. Asghari, M. Qandalee, Talanta 93 (2012) 37–43.
[22] J. Zhang, F. Zhang, H. Yang, X. Huang, H. Liu, J. Zhang, S. Guo, Langmuir 26 (2010) 6083–6085.
[23] L. Chen, H. Xie, J. Li, J. Solid State Electrochem. 16 (2012) 3323–3329.
[24] N. German, A. Ramanaviciene, J. Voronovic, A. Ramanavicius, Microchim. Acta 168 (2010) 221–229.
[25] W. Grosse, J. Champavert, S. Gambhir, G.G. Wallace, S.E. Moulton, Carbon 61 (2013) 467–475.
[26] H.B. Nguyen, T.T.T. Ngo, N.T. Nguyen, T.T.H. Dang, P.Q. Do, X.N. Nguyen, X.P. Nguyen, H.K. Phan, N.M. Phan, Adv. Nat. Sci. Nanosci. Nanotechnol. 3 (2012) 025011.
[27] M.M. Rahman, A. Ahammad, J.-H. Jin, S.J. Ahn, J.-J. Lee, Sensors 10 (2010) 4855–4886.
[28] X. Tu, Y. Zhao, S. Luo, X. Luo, L. Feng, Microchim. Acta 177 (2012) 159–166.
[29] Q. Xu, S.-X. Gu, L. Jin, Y.-e. Zhou, Z. Yang, W. Wang, X. Hu, Sensors Actuators B Chem. 190 (2014) 562–569.
[30] D. Zhai, B. Liu, Y. Shi, L. Pan, Y. Wang, W. Li, R. Zhang, G. Yu, ACS Nano 7 (2013) 3540–3546.
[31] K. Balasubramanian, M. Burghard, Small 1 (2005) 180–192.
[32] C. Garcia-Galan, Á. Berenguer-Murcia, R. Fernandez-Lafuente, R.C. Rodrigues, Adv. Synth. Catal. 353 (2011) 2885–2904.
[33] J. Wang, Electroanalysis 17 (2005) 7–14.
[34] M.V. Jose, S. Marx, H. Murata, R.R. Koepsel, A.J. Russell, Carbon 50 (2012) 4010–4020.
[35] P. Sharma, S.K. Tuteja, V. Bhalla, G. Shekhawat, V.P. Dravid, C. Suri, Biosens. Bioelectron. 39 (2013) 99–105.
[36] Q. Zhang, S. Wu, L. Zhang, J. Lu, F. Verproot, Y. Liu, Z. Xing, J. Li, X.-M. Song, Biosens. Bioelectron. 26 (2011) 2632–2637.
[37] Y.-X. Huang, X.-W. Liu, J.-F. Xie, G.-P. Sheng, G.-Y. Wang, Y.-Y. Zhang, A.-W. Xu, H.-Q. Yu, Chem. Commun. 47 (2011) 5795–5797.
[38] X. Yang, J. Zhu, L. Qiu, D. Li, Adv. Mater. 23 (2011) 2833–2838.
[39] C. Shan, H. Yang, D. Han, Q. Zhang, A. Ivaska, L. Niu, Biosens. Bioelectron. 25 (2010) 1070–1074.
[40] F. Cui, X. Zhang, J. Electroanal. Chem. 669 (2012) 35–41.
[41] Y. Chen, Y. Li, D. Sun, D. Tian, J. Zhang, J.-J. Zhu, J. Mater. Chem. 21 (2011) 7604–7611.
[42] W. Hong, H. Bai, Y. Xu, Z. Yao, Z. Gu, G. Shi, J. Phys. Chem. C 114 (2010) 1822–1826.
[43] X. Cao, Y. Ye, Y. Li, X. Xu, J. Yu, S. Liu, J. Electroanal. Chem. 697 (2013) 10–14.
[44] Y. Zhang, A. Yang, X. Zhang, H. Zhao, X. Li, Z. Yuan, Colloids Surf. A Physicochem. Eng. Asp. 436 (2013) 815–822.
[45] X. Dong, W. Huang, P. Chen, Nanoscale Res. Lett. 6 (2011) 60.
[46] I. Chowdhury, M.C. Duch, N.D. Manuskhani, M.C. Hersam, D. Bouchard, Environ. Sci. Technol. 47 (2013) 6288–6296.
[47] H. Wang, Y.H. Hu, J. Colloid Interface Sci. 391 (2013) 21–27.
[48] X. Zhang, M.R. Servos, J. Liu, J. Am. Chem. Soc. 134 (2012) 9910–9913.
[49] W.S. Hummers Jr., R.E. Offeman, J. Am. Chem. Soc. 80 (1958) 1339-1339.
[50] D. Li, M.B. Mueller, S. Gilje, R.B. Kaner, G.G. Wallace, Nat. Nanotechnol. 3 (2008) 101–105.
[51] G. Titelman, V. Gelman, S. Bron, R. Khalfin, Y. Cohen, H. Bianco-Peled, Carbon 43 (2005) 641–649.
[52] D.C. Marcano, D.V. Kosynkin, J.M. Berlin, A. Sinitskii, Z. Sun, A. Slesarev, L.B. Alemany, W. Lu, J.M. Tour, ACS Nano 4 (2010) 4806–4814.
[53] G.L. Li, G. Liu, M. Li, D. Wan, K. Neoh, E. Kang, J. Phys. Chem. C 114 (2010) 12742–12748.
[54] Y. Xu, K. Sheng, C. Li, G. Shi, J. Mater. Chem. 21 (2011) 7376–7380.
[55] X. Yang, M. Xu, W. Qiu, X. Chen, M. Deng, J. Zhang, H. Iwai, E. Watanabe, H. Chen, J. Mater. Chem. 21 (2011) 8096–8103.
[56] J. Huang, L. Zhang, B. Chen, N. Ji, F. Chen, Y. Zhang, Z. Zhang, Nanoscale 2 (2010) 2733–2738.
[57] X. Liu, M. Atwater, J. Wang, Q. Huo, Colloids Surf. B Biointerfaces 58 (2007) 3–7.
[58] Y. Oztekin, A. Ramanaviciene, Z. Yazicigil, A.O. Solak, A. Ramanavicius, Biosens. Bioelectron. 26 (2011) 2541–2546.
[59] C. Shan, H. Yang, J. Song, D. Han, A. Ivaska, L. Niu, Anal. Chem. 81 (2009) 2378–2382.
[60] B. Unnikrishnan, S. Palanisamy, S.-M. Chen, Biosens. Bioelectron. 39 (2013) 70–75.
[61] E. Laviron, J. Electroanal. Chem. Interfacial Electrochem. 101 (1979) 19–28.
[62] Q. Liu, X. Lu, J. Li, X. Yao, J. Li, Biosens. Bioelectron. 22 (2007) 3203–3209.
[63] H. Wang, X. Wang, X. Zhang, X. Qin, Z. Zhao, Z. Miao, N. Huang, Q. Chen, Biosens. Bioelectron. 25 (2009) 142–146.
[64] R.B. Rakhi, K. Sethupathi, S. Ramaprabhu, J. Phys. Chem. B 113 (2009) 3190–3194.
[65] X.-L. Luo, J.-J. Xu, Y. Du, H.-Y. Chen, Anal. Biochem. 334 (2004) 284–289.
[66] S. Palanisamy, S. Cheemalapati, S.-M. Chen, Mater. Sci. Eng. C 34 (2014) 207–213.
[67] J.C. Claussen, A. Kumar, D.B. Jaroch, M.H. Khawaja, A.B. Hibbard, D.M. Porterfield, T.S. Fisher, Adv. Funct. Mater. 22 (2012) 3399–3405.
[68] X. Wang, X. Zhang, Electrochim. Acta 112 (2013) 774–782.